American Journal of Energy Engineering
2026, Vol. 14, No. 3, pp. 117–125
https://doi.org/10.11648/j.ajee.20261403.13

Research Article

Study on the Particle Size and Specific Surface Area of Iron-Based Oxygen Carrier Modified Directionally by Fly Ash Powder

Haiwen Song[1], Bing Qu[2], Wenjie Wang[1], Shuaicheng Wang[2], Jinxing Wang[2,*]

[1]College of Metallurgy and Energy, North China University of Science and Technology, Tangshan, China
[2]College of Civil and Architectural Engineering, North China University of Science and Technology, Tangshan, China

Abstract

Iron-based oxygen carriers are among the most widely used carriers in chemical-looping hydrogen production technology, yet their pore size and specific surface area remain critical factors limiting reaction efficiency. Meanwhile, the potential of fly ash—rich in silicon, aluminum, as well as sodium, potassium, and calcium—to enhance the reactivity of iron-based oxygen carriers represents a strategic approach toward transforming waste into valuable resources in coal-fired power plants. In this study, synthetic iron-based oxygen carriers were prepared via co-precipitation, with 2 wt% fly ash added for comparative analysis. BET results indicate that incorporating fly ash increases the specific surface area from 12.56 m^2/g to 27.45 m^2/g, while also improving total pore volume and mesopore content. XRD and SEM analyses reveal that fly ash does not alter the crystalline phase but instead acts as an inactive framework, suppressing abnormal crystal growth at high temperatures and locally creating voids that form a complex interwoven pore structure. Single-particle crushing pressure tests demonstrate that adding 2 wt% fly ash significantly enhances mechanical strength, contributing to greater structural stability. This work integrates performance improvement of iron-based oxygen carriers with comprehensive utilization of fly ash, providing valuable insights for further exploration and application of chemical-looping hydrogen production technology.

Keywords

Iron Based Oxygen Carriers, Pore Structure, Fly Ash, Specific Surface Area, Crystalline Phase Composition, Crushing Strength

1. Introduction

Chemical looping hydrogen production (CLHP) technology is currently a critical pathway for realizing low-carbon energy utilization. The "Medium and Long-Term Development Plan for the Hydrogen Energy Industry (2021–2035)" explicitly identifies novel green hydrogen production processes including chemical looping hydrogen production as key technical projects to be advanced [1]. Among various oxygen carriers,

*Correspondence: Jinxing Wang (wangruoguang860928@126.com)

Received: 10 June 2026; **Accepted:** 27 July 2026; **Published:** 26 August 2026

iron-based oxygen carriers are recognized as promising candidates for practical application owing to their advantages such as low cost and stable composition [2].

As the oxygen carrier in the chemical-looping hydrogen production technology, the recyclability and conversion efficiency of this component are crucial factors in evaluating the feasibility of the technology [3]. Gao et [4] addressed the issues of low specific surface area, insufficient activity, and low hydrogen production capacity of traditional iron-based oxygen carriers. They prepared iron-based oxygen carriers with mesoporous structural characteristics using the impregnation method. By precisely controlling the structure of the microporous network, they significantly increased the rate of redox reactions. The Li team [5] addressed the issue of grain melting and collapse in the high-temperature zone of iron-based oxygen carriers during repeated use. They utilized fly ash to provide an inert matrix and certain active elements, achieving the effect of reconfiguring the microporous structure within the oxygen carrier, thereby delaying the decline in performance caused by the increase in the number of cycles. The Wang team [6] started from the problems of slow oxygen mass transfer and insufficient reactions, and explored whether the alkaline components of fly ash could enhance the effect of iron-based oxygen carriers. They achieved the improvement of the oxygen carrier's performance by preparing samples with added alkaline elements. Chen Yu et al. [7] conducted research on the calcination process of the iron-cerium composite functional carrier prepared by co-precipitation method. They mainly focused on the influence mechanisms of temperature and holding time on the microstructure, crystal phase composition and redox properties of the carrier. By effectively adjusting these conditions, the catalytic performance and stability of the carrier were greatly enhanced. The Zhao team [8] focused on the integrity of pore shapes and proposed a method of regularly removing impurities to prevent problems such as pore collapse and blockage. Fan et al. [9] used coal gangue as the raw material base to explore the technical and economic evaluation of the chemical looping hydrogen production process based on coal gangue. They calculated the energy consumption, operating costs, income, and investment limits of the entire scheme, and proved the effectiveness of the hydrogen production process combining coal gangue with chemical looping in terms of economic benefits. Chen et al. [10] shifted their focus to improving the hydrogen production performance of iron-alloy composites through the use of fly ash. From the perspective of waste material recycling, they considered how fly ash, as a carrier for oxygen, could function in the process of chemical-loop hydrogen production. Based on this, they redesigned the improved performance compatibility of the oxygen carrier and systematically adjusted the relevant process parameters, thereby enhancing the operational reliability of the entire hydrogen production system and the unit energy consumption level. This led to a significant transformation of fly ash from being an unwanted waste to a functional material, fundamentally reducing the demand for raw materials.

In conclusion, when applying fly ash to the directional modification of the pore structure of iron-based oxygen carriers, a comprehensive evaluation is still required in terms of specific surface area, surface morphology, phase change, and resistance to fragmentation. Therefore, in this work, we synthesized 60% Fe_2O_3/40% Al_2O_3 using the coprecipitation method with 2 wt% fly ash modification, and compared it with the control group that did not add fly ash. We hope this will provide a reference for the subsequent directional regulation and modification of iron-based oxygen carriers.

2. Sample Preparation

2.1. Experimental Material

The experimental materials selected for this work include $Fe(NO_3)_3 \cdot 9H_2O$ ($Fe(NO_3)_3 \cdot 9H_2O$, analytically pure), $Al(NO_3)_3 \cdot 9H_2O$ ($Al(NO_3)_3 \cdot 9H_2O$, analytically pure), ammonia solution with a concentration of 25% - 28% ($NH_3 \cdot H_2O$, analytically pure), polyvinyl alcohol (PVA), flyash, deionized water, etc.

For specific data, please refer to Table 1.

Table 1. *Experimental reagents.*

Reagent Name	specification parameter	use	Dosage (calculated based on 10g of finished oxygen carrier)	Notes
flyash	Main components (mass fraction) is SiO_2 48.6%, Al_2O_3 27.3%, CaO 6.8%, Fe_2O_3 4.2%, K_2O+Na_2O 3.5%, loss on ignition 9.6%	Modifier, auxiliary raw material	The dosage of 2% is 0.8 grams.	It needs to be pre-treated by calcination at 600°C for 2 hours.
$Fe(NO_3)_3 \cdot 9H_2O$	analytically pure, purity ≥ 99.0%	Active component precursor	30.3g (Fixed dosage)	Theoretical generation 6.0g Fe_2O_3
$Al(NO_3)_3 \cdot 9H_2O$	analytically pure, purity ≥ 99.0%	Carrier precursor	The amount of fly ash at 1% is 26.47g, at 2% is 23.53g, and at	Form a 4.0g Al_2O_3 + coal ash mixture in synergy with coal

Reagent Name	specification parameter	use	Dosage (calculated based on 10g of finished oxygen carrier)	Notes
			3% is 20.59g.	ash
polyvinyl alcohol (PVA)	analytically pure, Mw=1750±50	template	A 3% mass fraction is 7.5g. A 5% mass fraction is 12.5g. A 7% mass fraction is 17.5g.	Calculate based on the total mass of the mixed solution (approximately 250g)
ammonia	analytically pure, mass fraction 25%-28%	precipitant	8-10mL	Add dropwise to the solution until the pH reaches 9. Adjust the amount of fly ash as needed.
deionized water	specific conductance≤10μS/cm	solvent, lavation	The base mixture is 200 mL. The washing solution is 300 - 500 mL.	Wash until the filtrate contains no Cl^- (detected by silver nitrate test)

Among them, the preprocessing of fly ash is to remove the attached carbonaceous substances and desorb the alkaline ions such as Ca, K, and Na to achieve the precise control of the microstructure of the oxygen carrier in the next step. The raw coal ash is added to the ball mill for grinding for 30 minutes. It is passed through a 200-mesh sieve (with a corresponding aperture of 75 μm), and the large particles are all removed. The powder after sieving is sent to the muffle furnace. Under the condition that the constant temperature rate is maintained at 5°C/min, it is heated to 600°C and kept at this temperature for about 2 hours, then cooled back to room temperature. The high temperature effect causes the remaining non-combustible carbon to be oxidized and removed, while the original glass phase structure is damaged, and the ions originally existing in the powder in the form of alkali are transformed into soluble oxide states.

2.2. Manufacturing and Preparation Process

In this study, iron-based oxygen carriers were synthesized by the co-precipitation method [11, 12]. Al_2O_3 was used as the inert carrier, and fly ash was used as the active modifier component. Polyvinyl alcohol (PVA) was used as the spatial restrictor. The synthesis process of the samples is shown in Figure 1. The component ratio was set at 60% Al_2O_3, and the remaining proportion was distributed between Al_2O_3 and fly ash at 40%. According to this calculation, a certain amount of ferric nitrate and aluminum nitrate was dissolved into 200 mL of ultrapure water, heated to 20°C for magnetic stirring for 30 minutes until it completely turned into a uniform brownish-red solution. During this process, fly ash that had been surface-active treated was gradually added [13], with each addition of fly ash being 2%, and the same conditions were used for stirring for 60 minutes to ensure good dispersion. Then, a certain amount of 5% mass fraction PVA was added under the same conditions and stirred for another 60 minutes to form a stable suspension mixture. The precipitation process was gradually added with ammonia water at a speed of 1 mL/min. Throughout the process, the temperature remained constant at 20°C and 800 rpm. When the pH value of the system rose to 9, the addition of ammonia water was stopped, and the mixture was mixed for another 60 minutes to produce a brown gel-like precipitate. The precipitate was collected using a filter and washed with water multiple times until no Cl was detected in the solution (no white smoke was seen in the silver nitrate test). Then, anhydrous alcohol was added for one wash, and it was placed in a 105°C vacuum oven for 12 hours to obtain a dry gel-like pre-polymer. The pre-polymer was pressed into 3-5 mm-sized particles and placed in a furnace. It was heated at a rate of 5°C/min to 500°C and held for 3 hours to complete the decomposition of the catalyst and organic residues [14]. Then, the temperature was raised to 900°C and held for 3 hours to allow the crystal growth to complete. Finally, it was cooled back to the ambient temperature, and the product with a particle size of 0.2-0.3 mm was obtained by screening using a sieve.

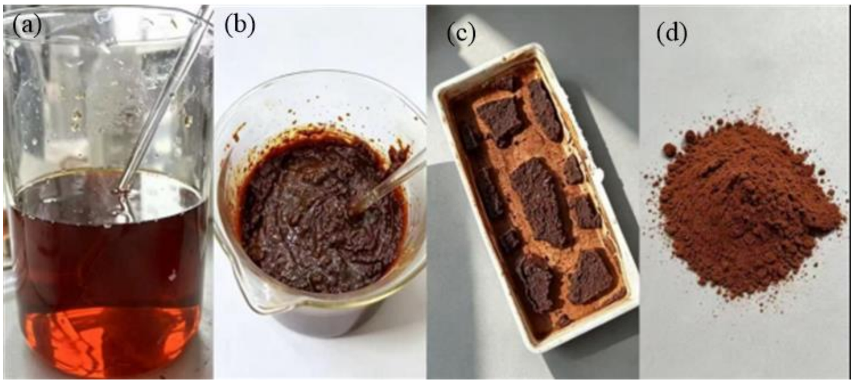

(a) mixed solution (b) The formed gel-like product (c) The dried precursor solid (d) The product after high-temperature calcination

Figure 1. *Sample photos from different preparation stages.*

3. Test Characterization

3.1. Analysis of Aperture and Specific Surface Area (BET)

The Aperture and Specific Surface Area Analyzer (BET, ASAP2460) is based on the physical adsorption of low-temperature nitrogen gas, combined with the BET multi-layer adsorption theory and the BJH mesoporous structure analysis method to determine the relevant numerical parameters such as the specific surface area, pore size distribution, and pore volume of the iron-based oxygen carrier. The testing process is completed under liquid nitrogen temperature (-196℃ / 77.3K). Under the low-temperature of liquid nitrogen, nitrogen molecules are subject to van der Waals forces and exhibit physical adsorption phenomena on the surface of the iron-based oxygen carrier. During the calcination process, various parameters such as the temperature gradient range of the electric furnace interior (300-1200℃), the duration of holding, and the heating rate are comprehensively adjusted. Based on the changes in BET specific surface area and BJH pore size during the calcination process, the trajectory of pore development corresponding to different calcination conditions can be traced, and the ideal calcination process range can be found, providing a reference for the precise design of pore structure.

3.2. X-ray Diffractometer (XRD)

The X-ray diffraction instrument (XRD, D8 ADVANCE) is based on Bragg's Law ($2d\sin\theta = n\lambda$), where d represents the distance between crystal planes, θ is the diffraction angle, n refers to the diffraction order, and λ is used to indicate the wavelength of the incident X-rays. The X-rays are generated by high-pressure accelerated electrons hitting metal anodes such as copper targets, emitting characteristic X-rays (typically CuKα, with λ = 0.15406 nm). Then, a monochromator separates out monochromatic X-ray beams with the same direction. After being directed towards the crystal sample surface of iron-based oxide carrier materials, the atoms (ions) arranged in a certain pattern within the crystal structure will scatter the incident light, causing interference phenomena between some of the incident light rays on different crystal planes due to the existence of positional differences, thereby generating distinct diffraction peaks.

3.3. Scanning Electron Microscope (SEM)

The scanning electron microscope (Scanning Electron Microscope, SEM, SU8010/SU8020) uses a high-energy focused electron beam to conduct point-by-point detection of the sample surface. It utilizes various signals generated between electrons and the measured substances to study and determine the micro-area morphology and structural information of the sample surface. The PHENOM G3 PRO is a desktop-type scanning electron microscope instrument equipped with a tungsten filament. Its operating principle is that the CeB6 filament (i.e., cerium boronized six filament, as indicated in the parameter values in the figure) emits electrons under the action of high pressure, and with the help of magnetic focusing lenses, it converges and accelerates into a beam of extremely fine electrons with a diameter of only a few nanometers. Through the scanning deflection coil, it controls its distribution to scan the regions on the sample surface in a certain pattern.

3.4. Particle Crushing Pressure Testing Equipment

The digital tensile tester (SM-500N) measures the crushing pressure of single particles through static compression. The core components are high-precision pressure sensors and a peak holding system. The single particle oxygen carrier is placed on a flat stage, and a uniform vertical pressure is applied at a constant speed. At the moment of particle crushing, the sensor records the maximum load, which represents the crushing pressure of the single particle, measured in Newtons (N). This equipment can accurately capture the critical force value for particle crushing, calculate the average and standard deviation of multiple sets of data, assess the stability of particle strength, and directly reflect the mechanical toughness and anti-flocculation ability of the oxygen carrier.

4. Results and Discussion

4.1. Comparison and Analysis of BET Surface Area and Pore Size Test Results

The BET method for conducting low-temperature nitrogen adsorption-desorption tests is one of the effective means for analyzing the pore structure of porous materials. Through this method, the specific surface area, total pore volume, average pore diameter, and pore size distribution can be accurately determined, thereby further obtaining the number of active sites in the oxygen carrier and the diffusion characteristics of gas molecules. The adsorption amount is shown in Figure 2. It can be observed that the addition of fly ash can significantly increase the adsorption amount of the iron-based oxygen carrier [15], with the maximum value being 2.5 times that of the sample without fly ash addition.

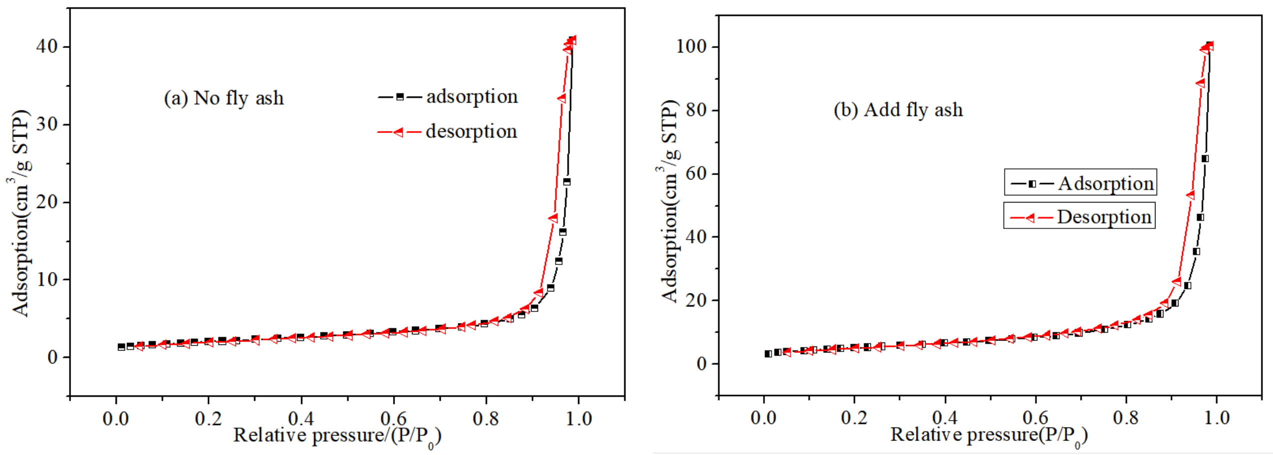

Figure 2. *Adsorption amounts under different relative pressures.*

During the high-temperature calcination process, the iron-based oxygen carrier will undergo crystallization and bonding, resulting in a large number of internal pores being sealed, thereby causing a significant reduction in surface area and pore volume. After adding fly ash, its original pore structure begins to show a trend of first increasing and then slowly decreasing. The differential pore volume distribution is shown in Figure 3.

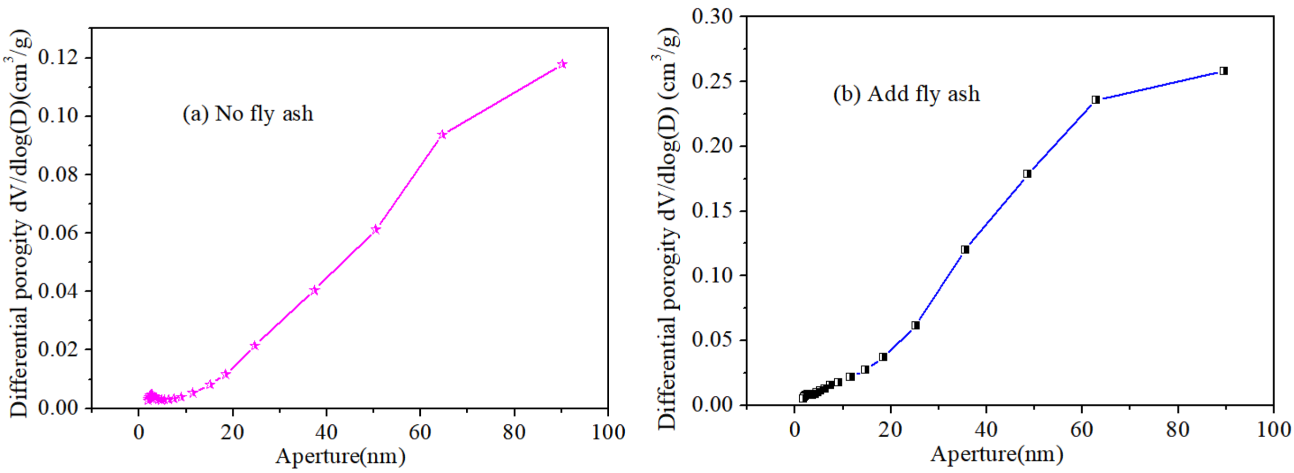

Figure 3. *Differential pore volume at different pore diameters.*

Tables 2 and 3 present the pore structure parameters and pore size distribution proportions after adding fly ash to the iron-based oxygen carrier. It can be observed that the iron-based oxygen carrier after adding fly ash has significant changes in terms of specific surface area, pore volume, etc. Its specific surface area has increased by 2.18 times, and the total pore volume has increased by 2.44 times. However, the impact on the average pore diameter is not significant, indicating that adding fly ash does not change the pore structure while increasing its specific surface area.

Table 2. Add the pore structure parameters of the iron-based oxygen carrier with fly ash.

Sample ID	fly ash replacement	BET specific surface area (m^2/g)	Total pore volume (cm^3/g)	mean pore size (nm)
Fe–0	0%	12.56	0.0896	28.54
Fe–2	2%	27.45	0.2183	27.40

Table 3. Add the pore size distribution ratio of the iron-based oxygen carrier with fly ash.

Sample ID	Porosity ratio (2–50 nm)	The proportion of large pores (>50 nm)	The proportion of micropores (<2 nm)
Fe–0	62.3%	35.7%	2.0%
Fe–2	86.5%	11.3%	2.2%

4.2. XRD Comparison and Analysis of Test Results

XRD can determine the state of the substance and estimate the grain size, thereby explaining how fly ash affects the arrangement of crystals. During the analysis, it was found that all samples had an α-Fe_2O_3 crystal structure and no other crystal phases appeared. This indicates that fly ash does not affect the formation of the main active crystals. The crystal phase characterization results are shown in Figure 4.

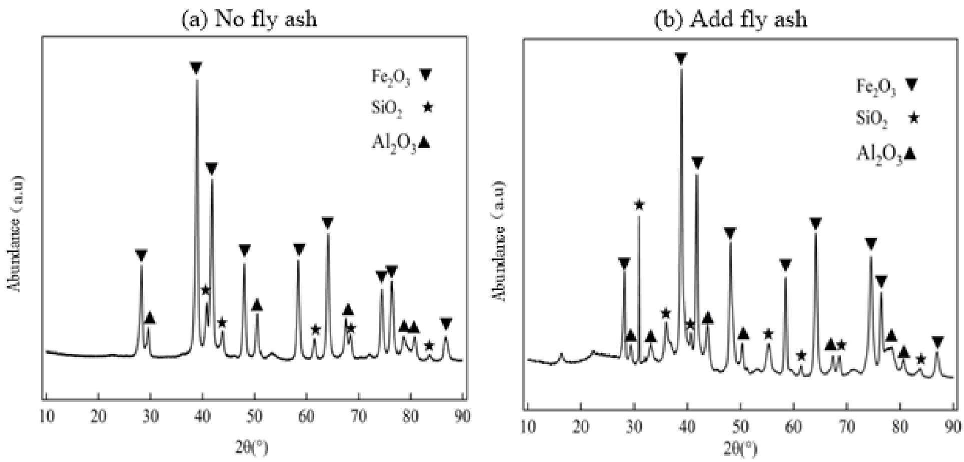

Figure 4. XRD test chart.

4.3. SEM Comparison and Analysis of Test Results

SEM characterization can clearly reflect the surface morphology of the oxygen carrier. Figure 5 shows the effects of the samples with added fly ash-based iron-based oxygen carriers and the control group. The surface of the samples without added fly ash is uniformly covered with small pores. In contrast, after adding fly ash, the size of the pores has significantly increased. This indicates that although adding fly ash does not directly change the basic framework of the synthesized iron-based oxygen carrier, it also affects the aggregation of the precipitated components during the synthesis process.

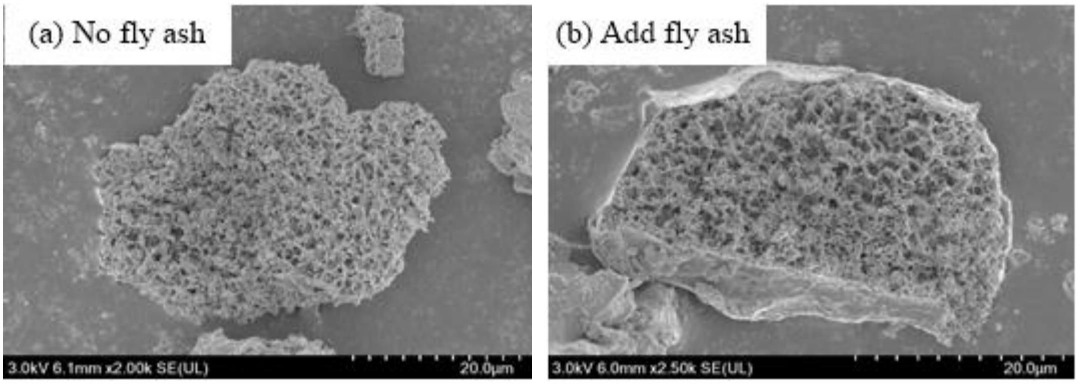

Figure 5. *Sample appearance picture.*

4.4. Comparison and Analysis of Carrier Crushing Pressure Test Results

Mechanical strength is a key indicator for maintaining the structural stability of iron-based oxygen carriers in chemical-looping hydrogen production reactors, and it directly affects their resistance to wear, pulverization, and cycle operation lifespan. To clarify the regulatory effect of fly ash content on the mechanical properties of the oxygen carrier, this study used a digital tensile tester to conduct single-particle crushing pressure tests on different samples. The test selected particles with a diameter of 0.2-0.3mm, and 20 particles were randomly tested in each group. The pressure was increased at a constant rate until the particles broke, the maximum crushing load was recorded and the average value was calculated. The results are shown in Table 4.

Table 4. *Single-particle crushing pressure of iron-based oxygen carriers with different amounts of fly ash content.*

Sample ID	fly ash replacement	Average crushing pressure/N	standard deviation/N
Fe–0	0%	18.6	1.2
Fe–2	2%	28.5	0.7

From the test results, it can be seen that the addition of fly ash has a significant impact on the mechanical strength of the oxygen carrier. The Fe–0 samples without fly ash addition undergo dense sintering after high-temperature calcination, with fewer internal defects but higher brittleness. Under external force, they are prone to brittle fracture, and the crushing pressure is only 18.6N. When the fly ash content is 2%, the average crushing pressure of the oxygen carrier reaches the maximum value of 28.5N, which is 53.2% higher than that of the pure iron-based sample. At the same time, the standard deviation is the smallest, and the strength stability is the best. The strengthening mechanism lies in: the SiO_2 and Al_2O_3 in fly ash interact with the matrix at high temperatures to form a stable silicate-aluminate rigid network, exerting a dispersion strengthening effect, effectively inhibiting abnormal grain growth; at the same time, the uniformly developed pore structure can disperse external stress, reducing the risk of stress concentration, enabling the material to maintain a porous structure while having high toughness and mechanical strength. The single-particle crushing pressure test results are highly consistent with the pore structure, microscopic morphology, and crystal phase analysis results, confirming that a 2% fly ash content can achieve the coordinated optimization of pore structure performance and mechanical strength, making the oxygen carrier more suitable for the industrial application requirements of chemical-looping hydrogen production.

5. Conclusion

This work focuses on the iron-based oxygen carrier system as the research object. It addresses the main difficulties that lead to the slow chemical chain hydrogen production rate, such as the asymmetric pore size distribution, low specific surface area, and the tendency to undergo sintering during high-temperature cycling. To overcome these issues, a method of using fly ash to precisely control the pore structure was proposed. A composite sample with a 2 wt% fly ash content was prepared using the co-precipitation method. The distribution was analyzed through a series of detection equipment such as the BET specific surface area pore size analyzer, XRD, and SEM. The control mode of fly ash on the pore evolution during the manufacturing process of the iron-based oxygen carrier and its applicability were elaborated in detail from aspects such as pore size, crystal structure, particle size, and surface shape. The specific conclusions are as follows:

(1) The content of fly ash has a significant guiding effect on the formation of the porous structure of iron-based oxides. When 2% fly ash is added, the active centers on the surface of the oxygen carrier are maximally stimulated. Under this condition, the BET specific surface area of the oxygen carrier is increased to 27.45 m^2/g, which is 2.18 times that of the original iron-based oxygen carrier; and the total pore volume also increases from the original 0.0896 cm^3/g to 0.2183 cm^3/g, which is 2.44 times that of the original iron-based oxygen carrier. At the same time, the average pore diameter does not change much.

(2) The XRD test results confirmed that the addition of fly ash did not cause any change in the crystal phase of the iron-based oxygen carrier, and it did not further lead to sintering problems. Furthermore, the SEM test results indicated that the presence of the inert components of fly ash was conducive to the formation of a more stable framework structure.

(3) The results of the crushing pressure test show that the mechanical properties of the material have been significantly improved after the addition of fly ash, with the compressive strength increasing by 53.2%. This further confirms the conclusion that the appropriate addition of fly ash can purposefully regulate the performance of iron-based oxygen carriers.

Abbreviations

CLHP	Chemical Looping Hydrogen Production
PVA	Polyvinyl Alcohol
XRD	X-ray Diffraction
SEM	Scanning Electron Microscope

Acknowledgments

Hebei Province Natural Science Foundation General Project: "Research on the Hierarchical Regulation of Iron-Based Lattice Oxygen Transfer in Calcium Matrix and Its Mechanism for Inhibiting Dioxin Generation from the Source (Project Number: E2025209014)"; Shijiazhuang city in Hebei university basic research project: "Study on the Mechanism of Regulating Iron-Based Lattice Oxygen Transfer by Affinity Adsorption and Inhibiting the Formation of Dioxins by Suppressing the Source (Project Number: 241791347A)".

Conflicts of Interest

The authors declare no conflicts of interest.

References

[1] National Energy Administration. Medium and Long-term Development Plan for Hydrogen Energy Industry (2021-2035) [R]. Beijing: National Energy Administration, 2024.

[2] YANG Liangnuo, LI Yilong, ZHOU Zheng, et al. Chemical-looping methane hydrogen production performance of Cu, La, Ce modified Fe_2O_3/Al_2O_3 oxygen carrier [J]. Journal of Fuel Chemistry, 2026, 54(4): 82-95.

[3] Davis M, Ouyang Y, Zhao L, et al. Challenges and prospects of fly ash-based oxygen carriers in chemical looping processes [J]. Renewable and Sustainable Energy Reviews, 2024, 185: 113624.

[4] Gao H, Liu M, Chen G, et al. Synthesis of mesoporous iron-based oxygen carriers via template-impregnation method for efficient hydrogen production [J]. International Journal of Hydrogen Energy, 2022, 47(8): 5210-5221.

[5] Li W, Zhang Q, Wang J, et al. Fly ash-modified iron-based oxygen carriers: Structure regulation and cyclic stability [J]. Chemical Engineering Journal, 2024, 475: 145432.

[6] Wang J, Li W, Zhang H, et al. Enhancing oxygen transfer efficiency of iron-based oxygen carriers using fly ash-derived alkaline elements [J]. Energy Conversion and Management, 2023, 286: 116987.

[7] Ouyang Y, Davis M, Gao H, et al. Influence of calcination conditions on the structure and performance of co-precipitated iron-cerium oxygen carriers [J]. Fuel Processing Technology, 2023, 241: 107328.

[8] Zhao L, Ouyang Y, Davis M, et al. Template removal strategies for mesoporous oxygen carriers: Efficiency and structure preservation [J]. Microporous and Mesoporous Materials, 2023, 345: 112389.

[9] Fan Y, Wang Z, Li C, et al. Techno-economic analysis of chemical looping hydrogen production from coal gangue [J]. Applied Energy, 2023, 334: 120658.

[10] Chen X, Li J, Zhang H, et al. Performance optimization of iron-based oxygen carriers using fly ash for chemical looping hydrogen production [J]. Fuel, 2022, 321: 123987.

[11] Zhao H, Wang J. Chemical-looping combustion of plastic wastes for *in situ* inhibition of dioxins. Combust. Flame. 2018; 191: 9-18.

[12] Wang J, Song H, Zhang Y, et al. Function pathways of CaO decoration on the internal transformation of PCDD/Fs isomers for chemical looping combustion of plastic waste. Energ Fuel, 2021, 35: 1741-1749.

[13] Lin S. L, Lee K. L, Wu J. L, et al. Effects of a quenching treatment on PCDD/F reduction in the bottom ash of a lab waste incinerator to save the energy and cost incurred from postthermal Treatment. Waste. Manage. 2019; 95: 316-324.

[14] Zhou S, Liu X, Wu Z, et al. Analysis of emissions reduction, spatial distribution, and reaction pathways of [formula omitted] during MILD combustion of biomass gasification gas [J]. Int J Hydrogen Energ, 2025,188,152111.

[15] Shi K, Feng J, Yang G, et al. Numerical study of NO_x emission reduction by MILD and air staged synergistic combustion in a new type of coke oven flue [J]. Int Commun Heat Mass, 2024, 159(PA): 107986.